Respiration Rate Measurement Under 1-D Body Motion Using Single Continuous-Wave Doppler Radar Vital Sign Detection System

Jianxuan Tu, *Student Member, IEEE*, Taesong Hwang, *Member, IEEE*, and Jenshan Lin, *Fellow, IEEE*

***Abstract*— Random body movement (RBM) is one of the most challenging issues in non-contact vital sign detection using Doppler radar technique. The large and irregular displacement of the human body could corrupt the vital sign signal and significantly degrade the accuracy of detection. Even the respiration rate (RR) sometimes cannot be measured accurately under RBM. In this paper, the characteristic of the frequency spectrum of the vital sign signal under body motion (the motion modulation effect) is analyzed. Based on that effect, an RR measurement method under one-dimensional (1-D) body motion is developed using only one non-contact continuous-wave (CW) Doppler radar vital sign detection system. The direction of body motion is extracted along with the new position of the respiration peaks in the frequency spectrum and RR can be calculated. Simulations of the theory using a model of the vital sign detection system are performed, followed by experiments to verify the theory. Experiments are performed on an actuator and a human subject by only one 5.8-GHz non-contact CW vital sign detection system. Under large 1-D body motion that has a displacement 5–10 times larger than the respiratory displacement, the proposed method successfully measures RR with only 7.15% error.**

***Index Terms*— Complex signal demodulation (CSD), motion modulation effect, non-contact continuous-wave (CW) Doppler radar vital sign detection system, one-dimensional (1-D) body motion, respiration rate (RR).**

I. Introduction

DOPPLER radar has been widely used in a large number of applications. Using microwave Doppler radar to detect physiological movements can be traced back to the early 1970s [1]. The non-contact vital sign detection systems transmit a single-tone continuous-wave (CW) signal, which is reflected back from a subject and carries the information of the physiological movements of the subject in its phase. The demodulated received signal contains the information of the respiration and heartbeat of the subject. This technique enables non-contact vital sign detection of humans and animals from a distance away. With this non-contact vital sign detection capability, the CW Doppler radar can be used in many different biomedical applications. Studies were conducted to demonstrate that it can monitor the respiration and heartbeat during overnight sleep with reasonable accuracy [2], making it possible to be used for sleep apnea monitoring [3]. Studies on humans in clinical environment also used this technique as the respiratory monitor and heartbeat monitor [4]–[6]. Moreover, recent studies have shown that Doppler radar could assist the radiation therapy [7]. It was also applied to monitor the vital signs of animals [8], [9]. Among many different demodulation methods, complex signal demodulation (CSD) [10] and arctangent demodulation [11] are two commonly used methods. Their advantages and disadvantages have been studied in [12]. The self and mutual injection-locking technique is also developed for vital sign detection [13].

Although a number of successful non-contact vital sign detection systems under different conditions and for different applications have been reported in the past [2]–[15], most of the studies focus on stationary subjects. One of the most challenging issues in non-contact vital sign detection is random body movement (RBM). Since non-contact vital sign detection is based on sensing tiny physiological movements of several millimeters to several centimeters, RBM, which has a displacement comparable to or larger than the chest wall displacement due to vital signs, is a substantial noise source that can destroy the signal of interest and significantly degrades the accuracy of detection. The noise produced by RBM prevents this technique from being widely applied.

Reference [10] reported a method using two radars to cancel RBM. By placing two radar systems facing the front and the back of the subject, respectively, the phase change produced by RBM has opposite signs in two radar systems. By adding the phase information after demodulation from two systems, the phase change caused by RBM can be cancelled. Reference [13] presented the self and mutual injection-locking technique and used two radar systems to cancel RBM as well. However, these methods have some drawbacks. First, they use multiple radar systems to cancel the phase change due to RBM, which increases the system complexity. Second, the alignment of different systems could be a potential bottleneck for accurate detection. Since the previous methods are based on a one-dimensional (1-D) model of RBM, if the two radar systems and the human body are not aligned well, the displacement due to RBM detected by different systems will have difference and cause error in RBM cancellation.

Manuscript received June 29, 2015; revised September 17, 2015, December 14, 2015, and April 21, 2016; accepted April 22, 2016. Date of publication May 17, 2016; date of current version June 2, 2016.

J. Tu and J. Lin are with the Department of Electrical and Computer Engineering, University of Florida, Gainesville, FL 32611 USA (e-mail: jxtu@ufl.edu; jenshan@ufl.edu).

T. Hwang was with the Department of Electrical and Computer Engineering, University of Florida, Gainesville, FL 32611 USA. He is now with Skyworks Solutions Inc., Newbury Park, CA 91320 USA (e-mail: taesonghwang@gmail.com).

Color versions of one or more of the figures in this paper are available online at http://ieeexplore.ieee.org.

Digital Object Identifier 10.1109/TMTT.2016.2560159

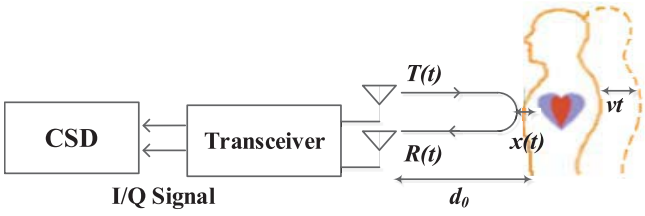

Fig. 1. Illustration of the detection setup of the motion modulation effect.

In order to study the RBM effect, this paper explores the vital sign detection under controlled body motion in a laboratory environment as a starting point. The characteristic of the frequency spectrum of the vital sign signal under 1-D body motion (the motion modulation effect) is analyzed in Section II. Body motion during vital sign measurement has a frequency-shift effect in the frequency spectrum of the vital sign signals. The direction and the amount of the frequency shift depend on the direction and the speed of the motion, respectively. Based on this characteristic, a method to detect the direction of 1-D body motion is developed, followed by a new method to detect the respiration rate (RR) under large 1-D body motion using only one non-contact CW Doppler radar system in Section III. Using the motion modulation effect, the respiration peaks in the shifted frequency spectrum can be located and RR can be calculated. System simulations are performed to verify the method and help to design the test system in Section IV. Based on the system simulation results, a 5.8-GHz non-contact CW Doppler radar vital sign detection system is designed and implemented. Experiments are performed to verify the performance of the proposed method and results are presented and analyzed in Section V, followed by a discussion and conclusion in Sections VI and VII.

II. Motion Modulation Effect

Fig. 1 illustrates the detection setup of the motion modulation effect. In a non-contact CW Doppler radar vital sign detection system, the transmitted signal is an unmodulated signal

$$T(t) = \cos[2\pi f t + \phi(t)] \tag{1}$$

with a carrier frequency f and an initial phase $\phi(t)$. It is transmitted to a subject at an initial distance of d_0 away. After hitting the human body, the phase of the transmitted signal is modulated by the physiological movement $x(t)$, which includes the chest wall displacement due to heartbeat and respiration. If the subject has 1-D body motion other than physiological movement, within a sufficiently short period of time, the motion in a single direction can be modeled as vt, where v is the speed of the motion. Neglecting the amplitude variation, the reflected signal captured by a radar receiver is represented as

$$R(t) \approx \cos\left[2\pi f t - \frac{4\pi d(t)}{\lambda} + \phi\left(t - \frac{2d_0}{c}\right)\right] \tag{2}$$

$$d(t) = d_0 \pm vt + x_h(t) + x_r(t) \tag{3}$$

where $d(t)$ is the combined motion, and $x_h(t)$ and $x_r(t)$ are respiratory and heartbeat displacement, respectively. The plus/minus signs before the vt term represent the direction of the motion. If the subject is moving toward the radar, which means the distance is getting shorter, a minus sign is applied and vice versa. After quadrature down-conversion and using the signals from the in-phase and quadrature-phase (I/Q) channels to perform CSD [10], the baseband signal can be expressed as

$$\begin{aligned} S(\mathrm{t}) &= \mathrm{I(t)} + \mathrm{jQ(t)} \\ &= \exp\left\{\mathrm{j}\left[-\frac{4\pi x_h(t)}{\lambda} - \frac{4\pi x_r(t)}{\lambda} \mp \frac{4\pi vt}{\lambda} + \phi\right]\right\} \end{aligned} \tag{4}$$

where ϕ represents the total residue phase. In order to analyze the vital signs, complex fast Fourier transform (FFT) is used to show the frequency spectrum of the baseband signal.

In (4), the minus sign before the vt term means the subject is moving away from the radar and vice versa. By using Bessel functions to extend the physiological movement terms in (4), we can get

$$\begin{aligned} S(\mathrm{t}) &= \exp\left\{\mathrm{j}\left[-\frac{4\pi x_h(t)}{\lambda} - \frac{4\pi x_r(t)}{\lambda} \mp \frac{4\pi vt}{\lambda} + \phi\right]\right\} \\ &= \mathrm{dc}_{IQ} + 2j[\mathrm{C}_{10}\sin(\omega_r \mathrm{t} + \phi_r) \\ &\quad + \mathrm{C}_{01}\sin(\omega_h \mathrm{t} + \phi_h) + .] \cdot \mathrm{e}^{j\phi} \cdot \exp\left(\mp\frac{4\pi vt}{\lambda}\right) \\ &\quad + 2[\mathrm{C}_{20}\cos(2\omega_r \mathrm{t} + 2\phi_r) \\ &\quad + \mathrm{C}_{02}\cos(2\omega_h \mathrm{t} + 2\phi_h) + .] \cdot \mathrm{e}^{j\phi} \cdot \exp\left(\mp\frac{4\pi vt}{\lambda}\right) \end{aligned} \tag{5}$$

where $x_h(t) = m_h \sin(\omega_h t + \phi_h)$ and $x_r(t) = m_r \sin(\omega_r t + \phi_r)$ are the periodic body movements due to heartbeat and respiration, λ is the wavelength of the carrier signal, ϕ is the total residual phase, $C_{ij} = J_i(4\pi m_r/\lambda) \cdot J_j(4\pi m_h/\lambda)$ determines the amplitude of every frequency component, $J_n(.)$ is the nth-order Bessel function of the first kind, and $dc_{IQ} = dc_I + j \cdot dc_Q$ is the combined dc component.

In (5), the signs before the sinusoidal terms are not important since they are periodic. However, the signs before the motion terms are crucial in the analysis because they indicate the direction of the motion and the direction of the frequency shift in the baseband frequency spectrum. The amount of frequency shift can be calculated as follows:

$$f_{\text{shifted}} = \frac{4\pi vt}{\lambda} \cdot \frac{1}{2\pi t} = \frac{2v}{\lambda}. \tag{6}$$

If the subject moves toward the radar, the original frequency spectrum will be shifted to the positive axis of the frequency spectrum by the amount of $2v/\lambda$. If the subject moves away from the radar, the original frequency spectrum will be shifted by the amount of $2v/\lambda$ to the negative axis. This characteristic, the motion modulation effect, was not mentioned in the previous studies [10], [13]. While studying vital sign detection under large 1-D body motion using a non-contact CW radar system, this effect needs to be considered to ensure useful information is not lost. For example, if the subject has backward body motion during the vital sign measurement and we only look at the frequency spectrum on the positive axis, the useful information on the negative axis is missed.

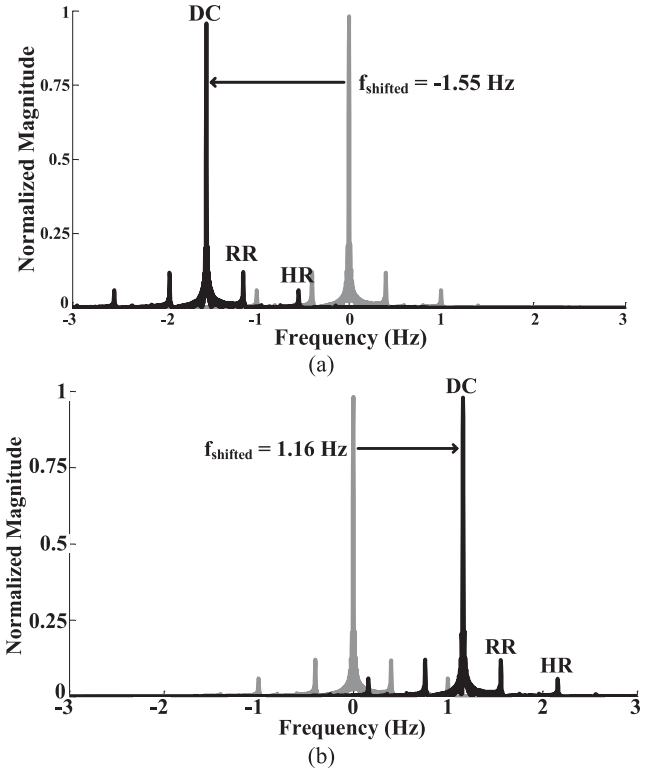

Fig. 2. Simulation results of using the motion modulation effect to detect motion direction of 1-D body motion. (a) Move backward. (b) Move forward.

Two issues need to be mentioned here. First, if we look at the frequency spectrum of the vital sign signal under RBM within a long-period time window, the motion modulation effect will not occur because the random motion in a long period of time cannot be modeled as (3). Second, if the speed v of the body motion is too large so that the corresponding shifted frequency $2v/\lambda$ is larger than half of the sampling frequency, the shifted frequency components of the vital sign signal will exceed the limit on one axis (positive or negative axis) and be folded onto the other axis (negative or positive axis) in the spectrum. For example, in the experiment, for a sampling frequency of 20 Hz and a carrier frequency of 5.8 GHz, the shifted frequency will exceed the limit when the speed v is larger than 25 cm/s. If the speed exceeds 25 cm/s, a higher sampling frequency should be used.

III. Motion Direction Detection and Vital Sign Measurement Under 1-D Body Motion

A. Motion Direction Detection

From the theory and analysis in Section II, using the characteristic of the frequency spectrum of vital sign signal under 1-D body motion, the motion direction can be detected. Fig. 2 shows the simulation results of the motion direction detection. The original signal is a vital sign signal expressed in (4) with RR of 0.4 Hz and heart rate (HR) of 1 Hz. The carrier frequency is 5.8 GHz. Both positive and negative axes of the frequency spectrum are shown. The light grey curve shows the original spectrum. The dark black curve shows the shifted spectrum. In the simulation shown in Fig. 2(a), the moving speed is set to be 4 cm/s and the motion direction is moving backward. Using (6), the amount of frequency shift is -1.55 Hz, which agrees with the simulation result. The highest peak at -1.55 Hz is the original dc component, which is shifted to the negative axis. The original respiration and heartbeat peaks are shifted to the left as well. In the simulation shown in Fig. 2(b), the moving speed is set to be 3 cm/s and the motion direction is moving forward, which creates a frequency shift of 1.16 Hz using (6). The highest peak at 1.16 Hz in Fig. 2(b) is the original dc component, which is shifted to the positive axis. From the theory and simulation result, the original respiration and heartbeat peaks are also shifted by the motion modulation effect. This observation is significant because it means that the detection of respiration and heartbeat under large 1-D body motion is possible using only one radar system. Here the large body motion means the magnitude of body motion is comparable or much larger than the chest wall displacement due to respiration, for example, 5–10 cm. One issue needs to be mentioned here. In Section II, body motion to a single direction is modeled as a movement with constant speed. However, in a real scenario, 1-D body motion could be an irregular back and forth movement or a single-direction movement with speed variation. In order to deal with the real scenario, we can divide a long-period time window of vital sign signal into several short-period time windows, where each short-period time window contains the movement toward one direction with a constant speed so that the model in Section II can still be used.

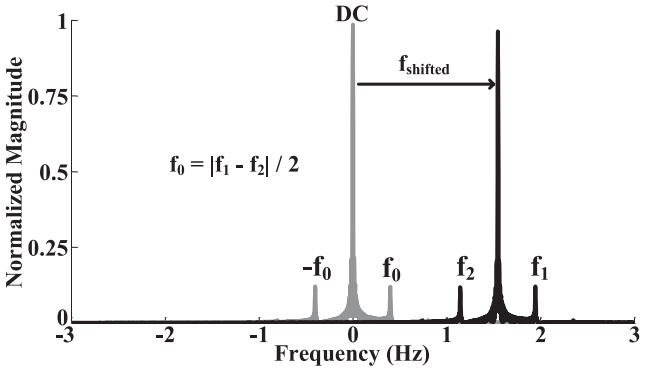

Fig. 3. Detection mechanism of the periodic movement frequency using motion modulation effect.

B. Vital Sign Measurement Under 1-D Body Motion

From the theory in Section II and the observation of the simulation result shown in Section III-A, the frequency of the vital signs under body motion can be detected. Fig. 3 illustrates the detection mechanism of the vital signs. The light grey curve shows the original spectrum. The dark black curve shows the shifted spectrum. To show the detection mechanism clearly, only the respiration signal is included in the simulation. The original frequencies of respiration components are f_0 and $-f_0$. During the motion, the spectrum is shifted by the amount of f_{shifted}, which can be calculated by (6). The new frequencies of the two peaks beside the shifted dc peak are f_1 and f_2. Thus, the frequency of the respiration signal can be calculated

as follows:

$$f_0 = \frac{|f_1 - f_2|}{2}. \tag{7}$$

By using the motion modulation effect, theoretically both HR and RR under 1-D body motion can be calculated. In a real scenario, however, the chest wall displacement due to heartbeat is too small as compared to the displacement due to respiration and body motion; therefore the heartbeat signal is easily corrupted by body motion and harmonic noise. Due to this reason, the measurement of HR is not included in the experiment part. A possible solution to measure HR under body motion could be identifying the harmonic peaks by advanced signal processing methods.

C. I/Q Mismatch Effect

I/Q mismatch takes place after an I/Q mixer. Several reasons can cause I/Q mismatch: the defect of a mixer integrated circuit (IC) and the capacitor mismatch in the baseband amplifier path. The theoretical analysis is shown below. If there is no I/Q mismatch, assume

$$\theta(t) = \frac{4\pi x_h(t)}{\lambda} + \frac{4\pi x_r(t)}{\lambda} + \frac{4\pi vt}{\lambda} \tag{8}$$

the signal from I/Q channels can be expressed as

$$\begin{cases} I(t) = \cos(\theta(t)) \\ Q(t) = \sin(\theta(t)) \end{cases} \tag{9}$$

the signal after CSD is shown in (10) as follows:

$$S(t) = I(t) + j \cdot Q(t) = \exp(j \cdot \theta(t)) \tag{10}$$

if I/Q mismatch appears as follows:

$$\begin{aligned} I(t) &= \cos(\theta(t)) = \frac{(\exp(j \cdot \theta(t)) + \exp(j \cdot -\theta(t)))}{2} \\ Q(t) &= \sin(\theta(t) + \theta_0) \\ &= \sin(\theta_0) \cdot \cos(\theta(t)) + \cos(\theta_0) \cdot \sin(\theta(t)) \\ &= \sin(\theta_0) \cdot \frac{(\exp(j \cdot \theta(t)) + \exp(j \cdot -\theta(t)))}{2} \\ &\quad + \cos(\theta_0) \cdot \frac{(\exp(j \cdot \theta(t)) - \exp(j \cdot -\theta(t)))}{(2j)} \end{aligned} \tag{11}$$

where θ_0 is the phase mismatch between the I and Q channels. The signal after CSD becomes

$$\begin{aligned} S(t) &= I(t) + j \cdot Q(t) \\ &= \frac{(\exp(j \cdot \theta(t)) + \exp(j \cdot -\theta(t)))}{2} \\ &\quad + j \cdot (\sin(\theta_0) \cdot \frac{(\exp(j \cdot \theta(t)) + \exp(j \cdot -\theta(t)))}{2} \\ &\quad + \frac{\cos(\theta_0) \cdot (\exp(j \cdot \theta(t)) - \exp(j \cdot -\theta(t)))}{(2j)} \\ &= \frac{1}{2} \exp(j \cdot \theta(t)) \cdot (1 + j \cdot \sin(\theta_0) + \cos(\theta_0)) \\ &\quad + \frac{1}{2} \exp(-j \cdot \theta(t)) \cdot (1 + j \cdot \sin(\theta_0) - \cos(\theta_0)). \end{aligned} \tag{12}$$

It can be observed from (12) that I/Q mismatch creates mirror frequency components in the frequency spectrum, the power of the mirrored peaks depends on the level of mismatch. Fig. 4 shows the simulation result of the frequency spectrum of the vital sign signal under 1-D body motion with I/Q mismatch. The original signal is the same as shown in Fig. 2. The phase mismatch between I and Q channels is 45°. One thing needs to be mentioned here. If the I/Q mismatch is greater than 90°, the magnitude of the mirror peak will be larger than the original peak, which leads to errors in detecting the motion direction. However, if the system is well designed, the I/Q mismatch should be less than 45°. The I/Q mismatch effect can be observed in the experiment results in Section V.

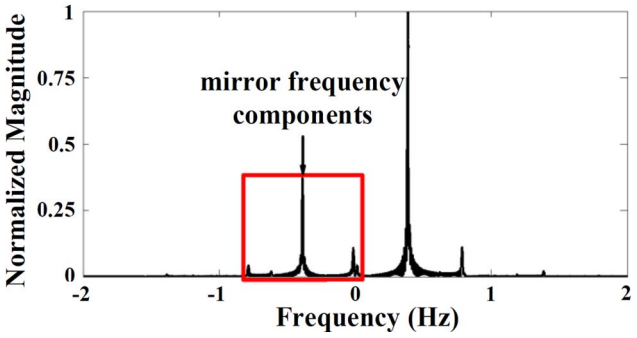

Fig. 4. Simulation result of the frequency spectrum of the vital sign signal under 1-D body motion with I/Q mismatch.

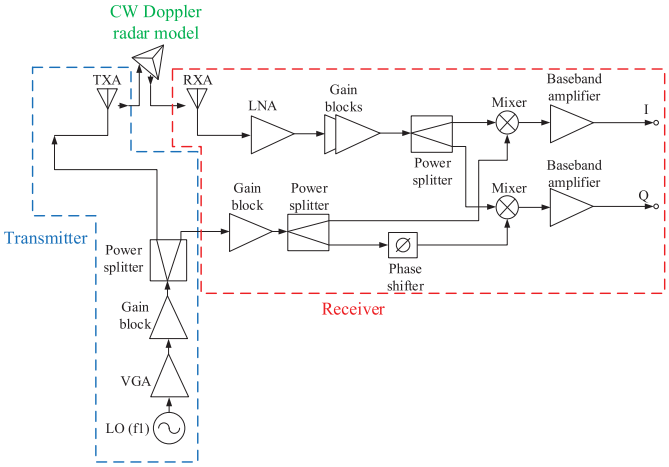

Fig. 5. Simulation block diagram of a vital sign detection system built in Agilent ADS.

IV. System Setup and Simulation

System-level simulations are performed in the Keysight Advanced Design System (ADS) to demonstrate the motion modulation effect in vital sign detection. Conditions of a human subject in a stationary state and on a track are simulated. A CW Doppler radar model is built and used to investigate and verify the theory.

A. Simulation Block Diagram of Vital Sign Detection System

Fig. 5 shows the simulation block diagram of the vital sign detection system in ADS. The detection system consists of a transmitter, a receiver, and a CW Doppler radar model. A local oscillator (LO) generates a 5.8-GHz single-tone signal source

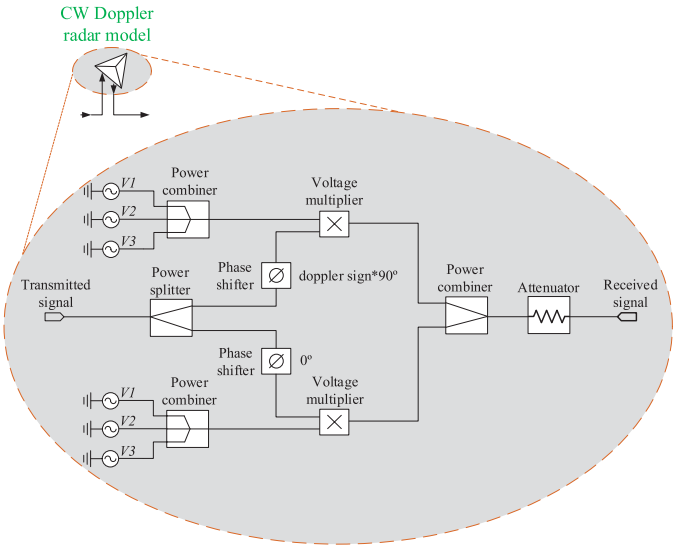

Fig. 6. Block diagram showing the components deployed in the Doppler radar model shown in Fig. 5.

and the signal source amplified by a variable gain amplifier (VGA) and a gain block is transmitted by a transmitting antenna (TXA). The receiver has a direct down-conversion architecture, which eliminates the need for an image rejection filter and makes the system simple. The received signal is amplified by a low-noise amplifier (LNA) and gain blocks. A quadrature mixer is used to resolve the null-point issue [10]. The transmitted signal is used to down-convert the received RF signal to baseband.

Fig. 6 shows the components deployed in the CW Doppler radar model shown in Fig. 5. The Doppler radar model demonstrates the effect of the displacement of the subject. The Doppler radar model consists of power combiners, a power splitter, phase shifters, voltage multipliers, an attenuator that accounts for signal attenuation during transmission, and signal sources that emulate 1-D body motion (V1), heartbeat (V2), and respiration (V3). The upper and lower branches generate baseband I/Q components of 1-D body motion, heartbeat, and respiration using V1, V2, and V3, respectively. The amplitude and sign of the Doppler shift due to the subject motion are considered in the simulations. Furthermore, the amplitudes of respiration and heartbeat are calculated using the Bessel function of the first kind.

B. Spectral Analysis

A single-tone signal at 5.8 GHz is transmitted and this signal is used to down-convert the received RF signal to baseband. The received baseband signal is analyzed to extract the vital signs of a subject. The phase of the baseband signal is modulated by the movement of the subject and contains the information of vital signs. The transmitted signal is expressed as (1).

We consider two different conditions: a person in a stationary state and a person moving on a track. For a person in a stationary state, the distance between the transmitter/receiver and the subject is fixed,

$$d_{\text{stationary}}(t) = d_0 \tag{13}$$

where d_0 is the initial distance between a transmitter/receiver and the subject. For a person moving on a track, the distance is described as (3). The received RF signal in the two conditions is described as (2). The displacement contains heartbeat and respiration information [10], which can be described as follows:

$$x(t) = m_h \sin \omega_h t + m_r \sin \omega_r t \tag{14}$$

where m_h and m_r are the amplitudes of heartbeat and respiration, and ω_h and ω_r are the angular frequencies of heartbeat and respiration. The baseband signals at the receiver in the two conditions can be described as follows:

$$B_{\text{stationary}}(t) \approx B \sum_{k=-\infty}^{\infty} \sum_{l=-\infty}^{\infty} J_l\left(\frac{4\pi m_h}{\lambda}\right) J_k\left(\frac{4\pi m_r}{\lambda}\right) \times \cos\left(k\omega_r t + l\omega_h t - \frac{4\pi d_0}{\lambda} + \Delta\phi(t)\right) \tag{15}$$

$$B_{\text{track}}(t) \approx B \sum_{k=-\infty}^{\infty} \sum_{l=-\infty}^{\infty} J_l\left(\frac{4\pi m_h}{\lambda}\right) J_k\left(\frac{4\pi m_r}{\lambda}\right) \times \cos\left(k\omega_r t + l\omega_h t - \frac{4\pi d_0}{\lambda} + \Delta\phi(t)\right) \tag{16}$$

where $J_n(.)$ is the nth-order Bessel function of the first kind and $\Delta\phi(t)$ is the total residual phase noise. The phase shift $4\pi vt/\lambda$ is due to the movement of the subject on a track.

C. Simulation Results

When a person is in a stationary state, 1-D body motion (V1) is zero. The parameters of the components used in the simulations are based on a vital sign detection system we have built. The parameters are adjusted to meet the link budget requirement. Envelope simulations in ADS are performed to demonstrate the vital sign detection system in the two conditions.

The transmitted power level is set to be about 10.5 dBm. The frequencies of heartbeat and respiration of the subject in a stationary state are set to be 0.2 and 1 Hz, respectively. In order to calculate the amplitudes of heartbeat and respiration, the Bessel function $j_n(n, x)$ in ADS is used in the simulations. The function $j_n(n, x)$ in ADS computes the Bessel function of the first kind and returns a real number where n is the order and x is the value of $4\pi m_h/\lambda$ or $4\pi m_r/\lambda$. The values of m_r and m_h used in the simulations are 1 and 0.08 cm, respectively. Fig. 7 shows the spectra of the transmitted signal $T(t)$ and received signal $B(t)$ when the subject is in a stationary state ($d_{\text{stationary}}(t) = d_0 = 1.5$ m). The power of the transmitted signal is 10.594 dBm. From the spectrum of the received signal after LNA in Fig. 7(b), the frequencies of respiration and heartbeat are well detected in the simulations. The spectrum is plotted by subtracting RF carrier frequency in the x-axis. The intermodulation and harmonic terms can be calculated using (15) and be observed in Fig. 7(b).

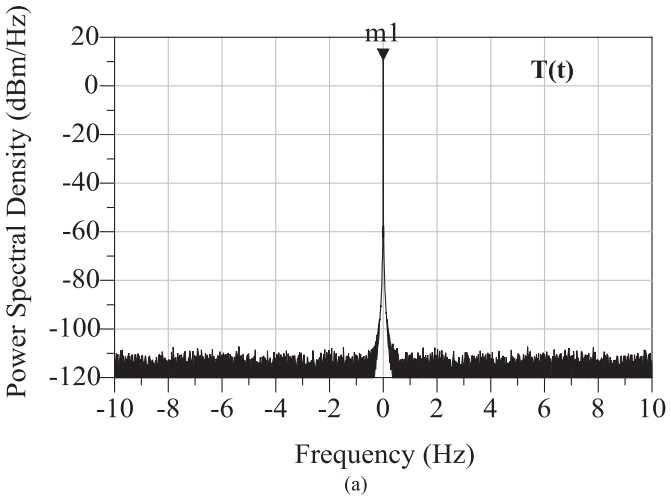

Fig. 7. Spectra of the transmitted signal and received signal when the subject is in a stationary state. (a) Spectrum of the transmitted signal $T(t)$ with a power of 10.594 dBm at marker m1. (b) Normalized spectrum of the received signal after LNA. Marker m1: respiration peak at 0.2 Hz. Marker m2: heartbeat peak at 1 Hz. Other peaks are intermodulation and harmonic terms.

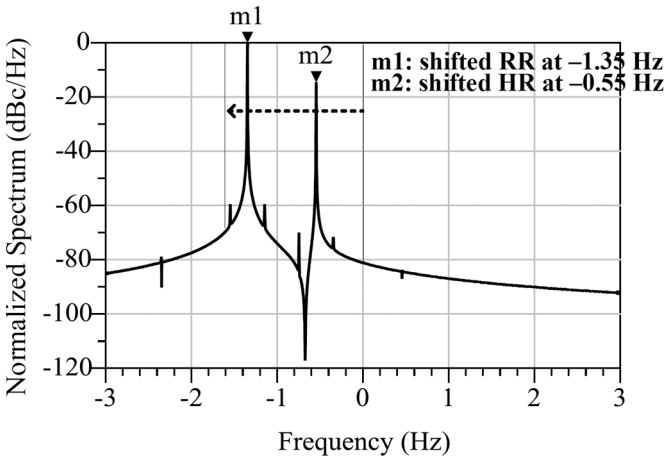

Fig. 8. Normalized spectrum of the received signal after LNA when the subject is moving away from the transmitter/receiver. Marker m1: shifted respiration peak at $0.2 - 1.55 = -1.35$ Hz. Maker m2: shifted heartbeat peak at $1 - 1.55 = -0.55$ Hz. The dashed arrow indicates RF carrier is shifted by -1.55 Hz.

Fig. 8 shows the normalized spectrum of the received signal after the LNA when the subject is moving away from a transmitter/receiver. The spectrum is also plotted by subtracting

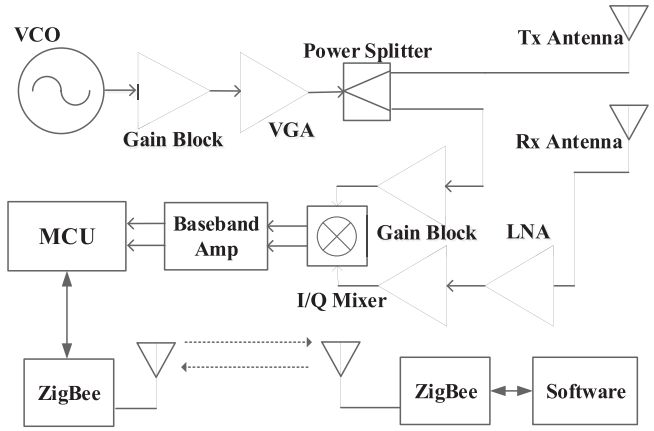

Fig. 9. Block diagram of the 5.8-GHz non-contact CW Doppler radar vital sign detection system.

RF carrier frequency in the x-axis. The movement speed is set to be 4 cm/s. From Fig. 8, it can be observed that the respiration and heartbeat peaks are shifted to the negative axis of the spectrum, which agrees with the analysis in Section III. We can observe that the shifted frequencies of respiration and heartbeat peaks are at -1.35 and -0.55 Hz, which are shifted by 1.55 Hz due to the movement $\pm vt$ on a track. The result agrees with the theoretical calculation results using (6),

$$\mp f = \mp\frac{2v}{\lambda} = \mp\frac{2(0.04)}{0.0517} \approx \mp 1.55 \text{ Hz}. \tag{17}$$

Comparing the ADS system simulation result in Fig. 8 with the theoretical analysis in Fig. 2(a), several differences should be mentioned. First, the dc term caused by direct coupling between transmitting and receiving antennas and background reflections is not simulated in the system simulation. Second, only a single-sideband modulated RF signal is used in the ADS system simulation. As a result, Fig. 8 only shows the modulated signal on the right side of the carrier.

V. Experiment Results

After the analysis and simulation, experiments were performed in the laboratory environment using only one 5.8-GHz non-contact CW Doppler radar vital sign detection system to verify the theory and simulation in Sections III and IV. The system was designed and implemented based on the simulation in Section IV. Fig. 9 illustrates the block diagram of the system. Fig. 10 shows photographs of the fabricated board (16.1 cm $\times$ 7.2 cm) and the test setup. The two-by-two patch antenna has a gain of around 6 dB. The half-power beamwidth (HPBW) is around 60° to ensure coverage and reduce the cluttering noise. A VGA is implemented to control the transmitted power for different measurement conditions. The transmitted power can be varied within 11–19 dBm. The I/Q mixer uses the transmitted signal as the LO to generate the I/Q signal for CSD. The micro-controller unit (MCU) has a built-in A/D convertor (ADC) to digitize the detected signal and generates control signals for the ZigBee module and VGA. The total power consumption of the circuit board is around 3 W. The design of the fabricated radar system board and component specifications are described in more details in [16]. The experiments were first performed on an

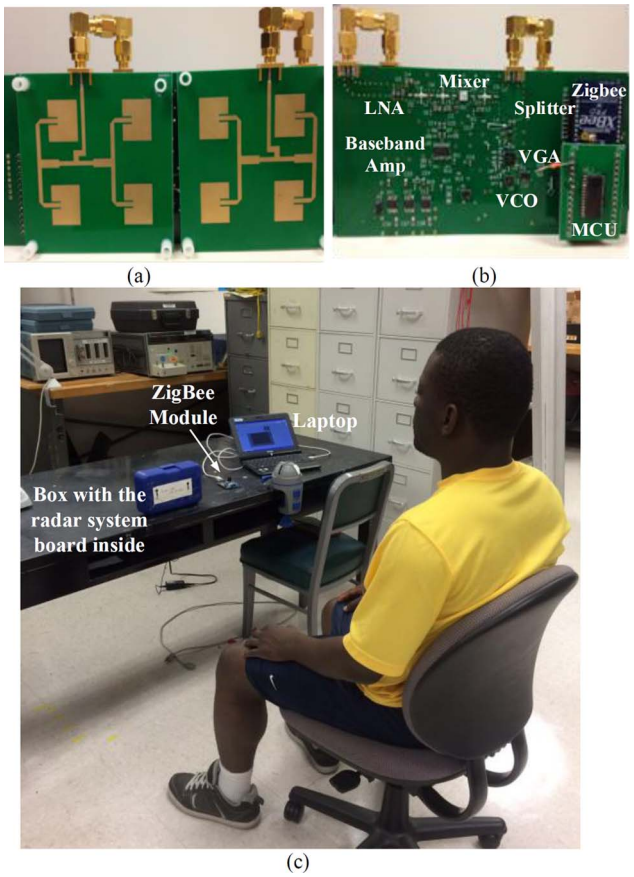

Fig. 10. Photographs of the radar system board and the test setup. (a) Front view. (b) Back view. (c) Test setup of the human test.

actuator and then on a human subject. For each kind of subject, typical measurement results are first presented and analyzed to compare with the simulation results, followed by statistical data to verify the performance of the method.

A. Actuator Test Results

The subject is a square plate with an aluminum foil on the surface fastened to an actuator (T-LA60A-S) vibrating at a certain frequency. The actuator was fastened on a cart and facing the radar system. The large motion was emulated by pulling and pushing the cart back and forth slowly in the direction, which was perpendicular to the surface of the reflecting plate. The actuator vibrated at 0.4 Hz. The motion directions were recorded during the experiments. Fig. 11 shows two of the experiment results of the actuator test. Fig. 11(a) shows the frequency spectrum of an experiment under the condition that the subject moved backward. The spectrum shows that the original frequency components are shifted to the negative axis of the spectrum. The direction detected agrees with the record. Fig. 11(b) shows another experiment result of the motion direction detection. From the record, the subject was moving toward the radar. It can be observed from the frequency spectrum that the frequency components are shifted to the positive axis, which means the subject moves toward the radar and the detection result agrees with record. Since both results use a 5-s time window, the resolution of the frequency

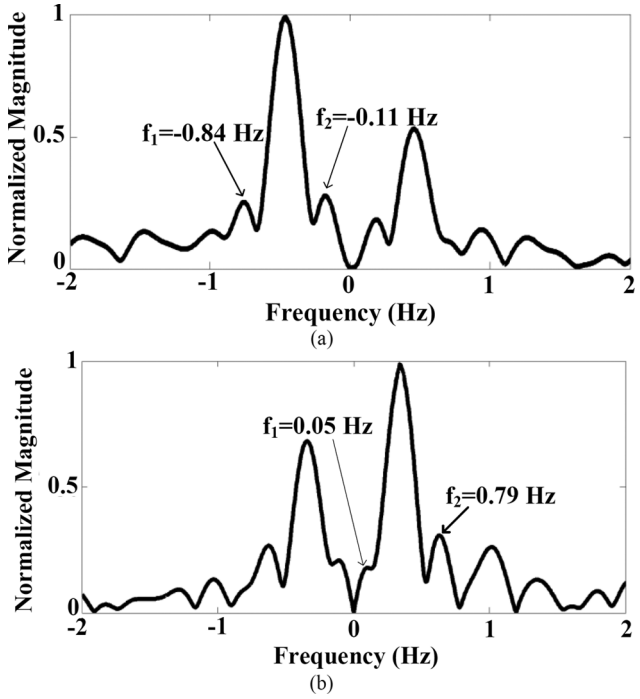

Fig. 11. Two typical experiment results (spectra) of the actuator test. (a) Move backward. (b) Move forward.

spectrum is low. However, it can be observed from Fig. 11 that the results agree with the theory and simulation. The direction of movement and speed of movement can be extracted from the frequency spectrum. The I/Q mismatch effect, which is mentioned in Section III-C, can also be observed. If we only look at the positive axis of the frequency spectrum and use the peak detection method to measure the frequency, either the frequency of the shifted dc component or the harmonics could be mistakenly identified as the vibration frequency and the result would be incorrect.

From the position of the dc peak, the speed of the movement is calculated using (6), which gives 1.2 cm/s from Fig. 11(a) and 0.88 cm/s from Fig. 11(b). Using (7), f_1 and f_2 are the highest peaks on the left and right sides of the shifted dc component. The frequency of the periodical movement is extracted as follows: in Fig. 11(a), the frequency is $(0.84 - 0.11)/2 = 0.365$ Hz; in Fig. 11(b), the frequency is $(0.79 - 0.05)/2 = 0.37$ Hz. The results are very close to 0.4 Hz.

Two sets of experiments were performed to verify the performance of the proposed method. The cart carrying the actuator moved back and forth slowly in the direction perpendicular to the surface of the reflecting plate. The frequencies of the actuator were set to be 0.5 and 1 Hz. For each frequency, several tests were performed. Fig. 12 shows the statistical results of the actuator test. The errors of the 0.5- and 1-Hz test set are 7.19% and 6.52%, respectively.

B. Human Test Results

For a human subject, the respiration frequency can be calculated using (7). Two sets of experiments, single-direction body movement test and bidirectional body movement test,

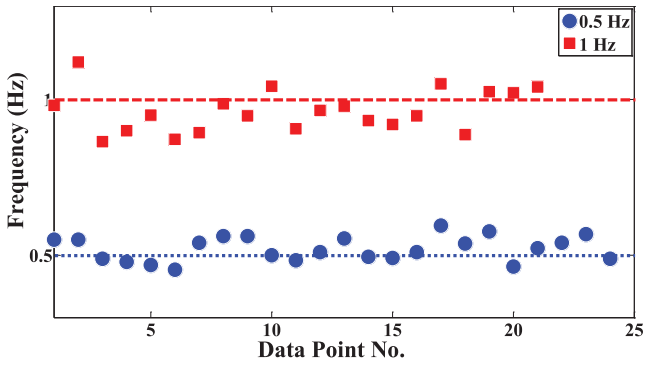

Fig. 12. Statistical results of actuator test: the frequencies of the actuator are set at 0.5 and 1 Hz.

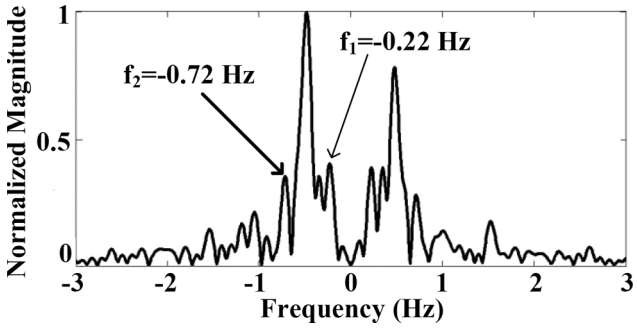

Fig. 13. Typical experiment result (spectrum) of single-direction body movement test.

were performed in a laboratory environment. Both experiment sets were performed under the condition that the amount of body motion displacement was either comparable to or much larger than the chest wall displacement due to respiration.

To perform the single-direction body movement test, the subject was asked to stay stationary and keep normal breathing for several seconds as a baseline for RR measurement. The subject was then asked to move back or forth slowly for several seconds. The speed of motion was controlled to be around 0.5 to 2 cm/s and the backward or forward movement lasted around 3–10 s. The vital sign data and motion direction were recorded during the experiments. Fig. 13 shows one of the experiment results in a 10-s window. The subject was moving backward. The extracted movement speed is about 1.2 cm/s. From the baseline measurement, RR is 0.25 Hz. Using (7), the measurement result of RR is $(0.72 - 0.22)/2 = 0.25$ Hz, which agrees with the baseline measurement.

In a real scenario of 1-D body motion, a subject moves back and forth unintentionally. In order to verify the performance of the proposed method, the subject was asked to move back and forth continuously to perform a bidirectional body movement test. In this set of experiments, each move to a single direction would last about 5 s. Before each bidirectional movement, the subject was again asked to stay stationary for several seconds to measure the baseline RR. To measure RR, the received data were divided into several time windows by recognizing the changes in the time and frequency domains due to the change in direction. Each time window contained the data of a single-direction motion. RR was extracted from each time window and then averaged.

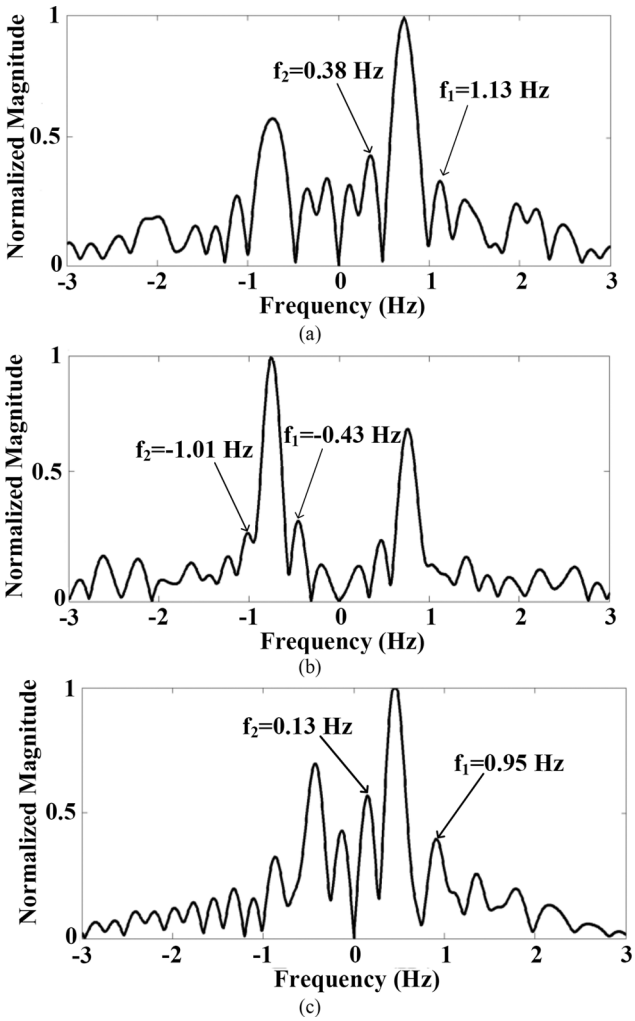

Fig. 14. Experiment results of a bidirectional body movement test. (a) 0–5 s, RR = 0.38 Hz. (b) 5-10 s, RR = 0.29 Hz. (c) 10-15 s, RR = 0.41 Hz.

Fig. 14 shows the results of one bidirectional body movement test. The total length of the time window is 15 s. The baseline measurement of RR is 0.32 Hz. Fig. 14(a)–(c) shows the spectra of 0–5, 5–10, and 10–15 s, respectively. From the spectra, the detected motion pattern is forward–backward–forward, which agrees with the record. RR is determined using the same method shown in Fig. 13 for each motion direction. The RR measurement result of this test set is the average of results from three motions, which gives $(0.38 + 0.29 + 0.41)/3 = 0.36$ Hz.

Table I shows the statistical results of the RR measurement under 1-D body motion. For each test set, the subject could move toward a single direction or move back and forth. The results of RR from each motion direction are averaged to obtain the RR measurement result for each test set and the error percentage for each test is calculated as follows:

$$\text{error percentage} = \frac{|\text{RR}_{\text{average}} - \text{RR}_{\text{baseline}}|}{\text{RR}_{\text{baseline}}} \times 100\%. \quad (18)$$

The total error percentage of human test is 7.15%, which is calculated by averaging the error percentages of all test sets. Several error sources should be listed here. First, RR during the motion could vary and be different from the baseline

TABLE I
RR MEASUREMENT RESULTS UNDER 1-D BODY MOTION

Test set number and RR baseline (stationary) measurement (Hz)	RR in motion (Hz)	Movement direction
I: 0.25	0.25	backward
	average: 0.25	
II: 0.24	0.256	Forward
	average: 0.256	
III: 0.25	0.275	forward
	0.269	backward
	0.257	forward
	average: 0.267	
IV: 0.32	0.38	forward
	0.29	backward
	0.41	forward
	average: 0.36	
V: 0.24	0.232	forward
	0.201	backward
	0.239	forward
	0.203	backward
	average: 0.219	
VI: 0.3	0.317	backward
	0.383	forward
	0.336	backward
	0.284	forward
	0.357	backward
	average: 0.335	
VII: 0.34	0.369	backward
	0.332	forward
	average: 0.351	

measurement. Second, the harmonics caused by RBM could degrade the accuracy. Third, the insufficient spectrum resolution could make it hard to locate the peaks precisely. Lastly, the clutter noise from the surrounding environment could raise the noise floor of the spectrum.

VI. DISCUSSION

The theoretical analysis, simulations, and experiments in the previous sections present a new method to measure RR under 1-D body motion using only one non-contact CW Doppler radar vital sign detection system with reasonable accuracy. However, the study is based on several assumptions and has some limitations, which need to be discussed here.

First, the displacements of the chest wall due to heartbeat and respiration are modeled as single-tone sinusoidal signals. The reason is to simplify the analysis [10], [12]. In a real scenario, the displacements do not necessarily have sinusoidal waveforms. A real respiration displacement waveform can be decomposed to a fundamental tone and a series of harmonics. Each decomposed frequency component can be analyzed and extracted using spectral analysis, which is similar to the analysis of the fundamental tone in (5), and contributes to the harmonics of the fundamental tone.

Second, 1-D body motion in a single direction within a sufficiently short period of time is modeled as a constant-speed movement. In a real scenario, such as RBM that has complex characteristics, the speed of the body motion could be non-constant. If the speed of motion varies during a chosen time window, according to (6), the amount of shifted frequency will be varying, which leads to a broader Doppler-shifted tone or multiple Doppler-shifted tones. To deal with this issue, a shorter time window might be necessary to identify the variation of the speed and keep a relatively constant-speed motion in each time window. If the variation of the speed in a chosen time window is within a certain range, the constant-speed assumption can still hold for an acceptable detection error. The challenge is that, for a short-period time window, the frequency spectrum resolution might be insufficient to accurately identify the peaks in the spectrum, which could become the dominant source of error. However, since the proposed method is based on calculating the difference between the shifted peaks, even if a motion with complex characteristics causes broader peaks or multiple peaks, the proposed method could still get a reasonable result.

Third, the study assumes 1-D body motion. For a potential application in 2-D or 3-D body motion, the 1-D motion along the direction of the chest wall displacement and the method proposed in this paper can still be used. The potential challenge is that 2-D or 3-D body motion could make the 1-D motion along the direction of the chest wall displacement more complex and corrupt the vital sign displacement more severely.

Finally, since the proposed detection method is based on locating the peaks of the vital signs after the frequency shift, a heartbeat signal can easily be corrupted by the harmonics close to the heartbeat peaks. The sources of the harmonics could be body motion, RR, demodulation method, and the clutter noise from the environment [12]. Measuring HR accurately using the proposed method presents additional challenges. The detection of HR under body motion using a single radar system will need further study.

Since the proposed method has some limitations and needs further study, the suggested application in current development stage is for relatively stable environment, such as sitting in a chair or on a bench. In order to resolve the limitations of the proposed method, from the signal-processing perspective, a more advanced signal-processing method could be used to enhance the spectrum resolution and suppress the harmonics. From the system perspective, other hardware using different architectures, such as the injection-locking technique [13], beam-steering antenna [15], low-IF architecture [17], six-port radar [18], and frequency-modulated continuous wave (FMCW) radar [19], and different frequencies [20] can also be considered. Future solutions for the RBM problem could be combinations of innovative hardware architectures and advanced signal-processing techniques.

VII. CONCLUSION

This paper has studied the characteristics of the vital sign signal under 1-D body motion—the motion modulation effect. Based on this effect, this work presents a new method to simultaneously detect motion direction and measure RR under large 1-D body motion using only one CW Doppler radar. A theory was developed and the modeling and simulations of the vital sign detection system were performed. Experimental results on an actuator and a human subject verified the theory and

simulation. RR under 1-D body motion can be successfully measured using the proposed method while HR measurement under RBM needs further study. The study of the motion modulation effect could be a starting point for future solutions for the RBM effect.

REFERENCES

[1] J. C. Lin, "Noninvasive microwave measurement of respiration," *Proc. IEEE*, vol. 63, no. 10, p. 1530, Oct. 1975.

[2] C. Li, J. Lin, and Y. Xiao, "Robust overnight monitoring of human vital signs by a non-contact respiration and heartbeat detector," in *28th Annu. IEEE Int. Eng. Med. Biol. Soc. Conf.*, 2006, pp. 2235–2238.

[3] N. A. Fox, C. Heneghan, M. Gonzalez, R. B. Shouldice, and P. D. Chazal, "An evaluation of a non-contact biomotion sensor with actimetry," in *Annu. IEEE Int. Eng. Med. Biol. Soc. Conf.*, 2007, pp. 2664–2668.

[4] W. Massagram, V. M. Lubecke, and O. Boric-Lubecke, "Microwave non-invasive sensing of respiratory tidal volume," in *Annu. IEEE Int. Eng. Med. Biol. Soc. Conf.*, 2009, pp. 4832–4835.

[5] A. D. Droitcour *et al.*, "Non-contact respiratory rate measurement validation for hospitalized patients," in *Annu. IEEE Int. Eng. Med. Biol. Soc. Conf.*, 2009, pp. 4812–4815.

[6] O. Postolache, P. S. Girao, E. Lunca, P. Bicleaknu, and M. Andrusca, "Unobtrusive cardio-respiratory monitoring based on microwave Doppler radar," in *Int. Elect. Power Eng. Conf. and Expo.*, 2012, pp. 597–600.

[7] C. Gu *et al.*, "Accurate respiration measurement using DC-coupled continuous-wave radar sensor for motion-adaptive cancer radiotherapy," *IEEE Trans. Biomed. Eng.*, vol. 59, no. 11, pp. 3117–3123, Nov. 2012.

[8] A. Singh, S. Lee, M. Butler, and V. M. Lubecke, "Activity monitoring and motion classification of the lizard *chamaeleo jacksonii* using multiple Doppler radars," in *Annu. IEEE Int. Eng. Med. Biol. Soc. Conf.*, 2012, pp. 4525–4528.

[9] N. Hafner, J. Drazen, and V. Lubecke, "Fish heart rate monitoring by body-contact Doppler radar," *IEEE Sensors J.*, vol. 13, no. 1, pp. 408–414, Jan. 2012.

[10] C. Li and J. Lin, "Complex signal demodulation and random body movement cancellation techniques for non-contact vital sign detection," in *IEEE MTT-S Int. Microw. Symp. Dig.*, Jun. 2008, pp. 567–570.

[11] B. Park, O. Boric-Lubecke, and V. M. Lubecke, "Arctangent demodulation with DC offset compensation in quadrature Doppler radar receiver systems," *IEEE Trans. Microw. Theory Techn.*, vol. 55, no. 5, pp. 1073–1079, May 2007.

[12] J. Tu and J. Lin, "Respiration harmonics cancellation for accurate heart rate measurement in non-contact vital sign detection," in *IEEE MTT-S Int. Microw. Symp. Dig.*, 2013, pp. 1–3.

[13] F.-K. Wang, T.-S. Horng, K.-C. Peng, J.-K. Jau, J.-Y. Li, and C.-C. Chen, "Single-antenna doppler radars using self and mutual injection locking for vital sign detection with random body movement cancellation," *IEEE Trans. Microw. Theory Techn.*, vol. 59, no. 12, pp. 3577–3587, Dec. 2011.

[14] C. Li, J. Ling, J. Li, and J. Lin, "Accurate Doppler radar noncontact vital sign detection using the RELAX algorithm," *IEEE Trans. Instrum. Meas.*, vol. 59, no. 3, pp. 687–695, Mar. 2010.

[15] C.-M. Nieh and J. Lin, "Adaptive beam-steering antenna for improved coverage of non-contact vital sign radar detection," in *IEEE MTT-S Int. Microw. Symp. Dig.*, Tampa, FL, USA, Jun. 2014, pp. 1–3.

[16] J. Tu and J. Lin, "Fast acquisition of heart rate in noncontact vital sign radar measurement using time-window-variation technique," *IEEE Trans. Instrum. Meas.*, vol. 65, no. 1, pp. 112–122, Jan. 2016.

[17] C. Wei and J. Lin, "Digitally assisted low IF architecture for noncontact vital sign detection," in *IEEE MTT-S Int. Microw. Symp. Dig.*, Phoenix, AZ, USA, Jun. 2015, pp. 1–4.

[18] G. Vinci *et al.*, "Six-port radar sensor for remote respiration rate and heartbeat vital-sign monitoring," *IEEE Trans. Microw. Theory Techn.*, vol. 61, no. 5, pp. 2093–2100, May 2013.

[19] S. Ayhan, M. Pauli, T. Kayser, S. Scherr, and T. Zwick, "FMCW radar system with additional phase evaluation for high accuracy range detection," in *Proc. Eur. Radar Conf.*, Oct. 2011, pp. 117–120.

[20] T. Y. J. Kao, A. Y. K. Chen, Y. Yan, T.-M. Shen, and J. Lin, "A flip-chip-packaged and fully integrated 60 GHz CMOS micro-radar sensor for heartbeat and mechanical vibration detections," in *IEEE Radio Freq. Integr. Circuits Symp.*, 2012, pp. 443–446.

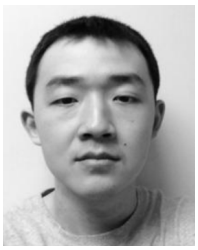

Jianxuan Tu (S'13) received the B.S. degree in information science and technology from Southeast University, Nanjing, China, in 2010, and the Ph.D. degree in electrical engineering from the University of Florida, Gainesville, FL, USA, in 2015.

His research interests include Doppler radar system and measurement algorithms for non-contact vital sign detection on humans and animals.

Dr. Tu is currently a Reviewer for the IEEE TRANSACTIONS ON INSTRUMENTATION AND MEASUREMENT.

Taesong Hwang (S'12–M'14) received the B.E. degree in electronic engineering from Dong-A University, Busan, Korea, in 2009, and the M.S. and Ph.D. degrees in electrical and computer engineering from the University of Florida, Gainesville, FL, USA, in 2011 and 2014, respectively.

He is currently with Skyworks Solutions Inc., Newbury Park, CA, USA, where he is involved in design of high-volume power-amplifier products and sub-systems for cellular handset applications. His research interests include high-efficiency linear power amplifiers, linearization techniques for power amplifiers, and transformers in an integrated passive device (IPD) scheme.

Dr. Hwang is currently a Reviewer for IEEE MICROWAVE AND WIRELESS COMPONENTS LETTERS, the IEEE TRANSACTIONS ON MICROWAVE THEORY AND TECHNIQUES, and the IEEE TRANSACTIONS ON CIRCUITS AND SYSTEMS—PART I: REGULAR PAPERS.

Jenshan Lin (S'91–M'94–SM'00–F'10) received the Ph.D. degree in electrical engineering from the University of California at Los Angeles (UCLA), Los Angeles, CA, USA, in 1994.

From 1994 to 2001, he was with AT&T Bell Laboratories (which later became Lucent Bell Laboraties), Murray Hill, NJ, USA, and from 2001 to 2003, with its spin-off Agere Systems. In July 2003, he joined the University of Florida, Gainesville, FL, USA, as an Associate Professor and became a Professor in August 2007. In the summer of 2006, he was a Visiting Professor with National Taiwan University. During the summer of 2010, he was a Visiting Researcher with NTT, Atsugi, Japan. In the summer of 2012, he was a Visiting Chair Professor with National Sun Yat-Sen University, Kaohsiung, Taiwan. In 2014, he was appointed as an Honorary Chair Professor of National Taiwan University of Science and Technology. He has authored or coauthored over 250 technical publications in refereed journals and conferences proceedings. He holds 15 U.S. patents. His research interests include sensors and biomedical applications of microwave and millimeter-wave technologies, wireless power transfer, wireless communication systems, and power amplifiers.

Dr. Lin has served on several committees of the IEEE Microwave Theory and Techniques Society (IEEE MTT-S). From 2006 to 2011, he was an elected Member of the IEEE MTT-S Administrative Committee (AdCom), where he served as the Chair of the Technical Coordinating Committee from 2010 to 2011. He is a Member of the IEEE MTT-S Technical Committees MTT-20 (Wireless Communications), MTT-23 (RFIC), and MTT-26 (Wireless Energy Transfer and Conversion). From 2006 to 2010, he was an Associate Editor for the IEEE TRANSACTIONS ON MICROWAVE THEORY AND TECHNIQUES. He is currently the Editor-in-Chief of the IEEE TRANSACTIONS ON MICROWAVE THEORY AND TECHNIQUES. He serves on the Editorial Advisory Board of the Cambridge University Press' "RF and Microwave Engineering Series." He has been a Member of several conference committees, including the IEEE MTT-S International Microwave Symposium (IMS), the Radio Frequency Integrated Circuits Symposium (RFIC), the Radio and Wireless Symposium (RWS), the International Wireless Symposium (IWS), and the Asia–Pacific Microwave Conference (APMC). He was the General Chair of the 2008 RFIC Symposium, the Technical Program Chair of the 2009 Radio and Wireless Symposium, and the General Co-Chair of the 2012 Asia–Pacific Microwave Conference. He was the recipient of the 1994 UCLA Outstanding Ph.D. Award, the 1997 Eta Kappa Nu Outstanding Young Electrical Engineer Honorable Mention Award, the 2007 IEEE MTT-S N. Walter Cox Award, and the National Chiao Tung University (NCTU) Distinguished Alumnus Award in 2016. He was also a five-time recipient of the University of Florida Technology Innovator Award from 2011 to 2015.